



## ISTITUTO NAZIONALE DI RICERCA METROLOGICA Repository Istituzionale

The linkup of mono-elemental solutions to the SI using INAA: a measurement procedure and the achievable uncertainty

This is the author's accepted version of the contribution published as:

*Original*

The linkup of mono-elemental solutions to the SI using INAA: a measurement procedure and the achievable uncertainty / D'Agostino, Giancarlo; Bergamaschi, Luigi; Di Luzio, Marco; Noordmann, Janine; Oddone, Massimo; Rienitz, Olaf. - In: JOURNAL OF RADIOANALYTICAL AND NUCLEAR CHEMISTRY. - ISSN 0236-5731. - 309:2(2016), pp. 777-786.

*Availability:*

This version is available at: 11696/51981 since: 2020-05-19T10:40:33Z

*Publisher:*

Springer

*Published*

DOI:10.1007/s10967-015-4676-2

*Terms of use:*

Visibile a tutti

This article is made available under terms and conditions as specified in the corresponding bibliographic description in the repository

*Publisher copyright*

SPRINGER

Copyright © Springer. The final publication is available at [link.springer.com](https://link.springer.com)

(Article begins on next page)

1

## **Title page**

2 Names of the authors: Giancarlo D'Agostino<sup>(1)</sup>, Luigi Bergamaschi<sup>(1)</sup>, Marco Di  
3 Luzio<sup>(1,2)</sup>, Janine Noordmann<sup>(3)</sup>, Massimo Oddone<sup>(2)</sup> and Olaf Rienitz<sup>(3)</sup>

4 Title: The linkup of mono-elemental solutions to the SI using INAA: a measurement  
5 procedure and the achievable uncertainty

6 Affiliation(s) and address(es) of the author(s): (1) Istituto Nazionale di Ricerca  
7 Metrologica (INRIM) - Unit of Radiochemistry and Spectroscopy, c/o Department of  
8 Chemistry, University of Pavia, via Taramelli 12, 27100 Pavia, Italy; (2) Department of  
9 Chemistry – Radiochemistry Area, University of Pavia, via Taramelli 12, 27100 Pavia,  
10 Italy; (3) Physikalisch-Technische Bundesanstalt (PTB), Bundesallee 100, 38116  
11 Braunschweig, Germany

12 E-mail address of the corresponding author: [g.dagostino@inrim.it](mailto:g.dagostino@inrim.it)

13

14 **The linkup of mono-elemental solutions to the SI using**  
15 **INAA: a measurement procedure and the achievable**  
16 **uncertainty**

17 D'Agostino G.<sup>1</sup>, Bergamaschi L.<sup>1</sup>, Di Luzio M.<sup>1,2</sup>, Noordmann J.<sup>3</sup>, Oddone M.<sup>2</sup> and  
18 Rienitz O.<sup>3</sup>

19 <sup>1</sup>*Istituto Nazionale di Ricerca Metrologica (INRIM), via Taramelli 12, 27100 Pavia, Italy*

20 <sup>2</sup>*Department of Chemistry, University of Pavia, via Taramelli 12, 27100 Pavia, Italy*

21 <sup>3</sup>*Physikalisch-Technische Bundesanstalt (PTB), Bundesallee 100, 38116 Braunschweig,*  
22 *Germany*

23 **Abstract**

24 The possibility of using neutron activation analysis to link up a secondary to a primary  
25 mono-elemental solution was investigated. A procedure was developed for the  
26 determination of the ratio between the mass fractions of two solutions. The use of a  
27 monitor element was essential to limit the effect of the non-uniformity of the neutron flux  
28 during irradiation. The proposed procedure was tested in the case of two molybdenum  
29 solutions having the same mass fraction. Although the experiment did not reach the goal,  
30 possible ways are suggested to reach the target expanded uncertainty of 0.1 %.

31 **Keywords**

32 Neutron activation analysis; metrological traceability; reference solution; molybdenum.

33 **Introduction**

34 Mono-elemental solutions with a mass fraction of  $1 \text{ g kg}^{-1}$  are being used in almost every  
35 chemical laboratory in social, medical and industrial fields to calibrate analytical  
36 measurements. The accuracy of those solutions is essential for the reliability and  
37 comparability of the applied analyses.

38 Due to the importance of these calibration solutions, traceability to the SI is necessary.  
39 Several national metrology institutes (NMIs) or designated institutes (DIs) provide  
40 traceability by the use of high purity solid materials ( $w_{\text{pur}} \geq 0.999 \text{ g g}^{-1}$ ) with completely  
41 known impurities (metals and non-metals), yielding a purity with an associated expanded  
42 uncertainty of less than 0.01 %. In some cases, the distribution of selected impurities  
43 among subsamples of the solid materials have been also investigated [1]. Based on these  
44 solid materials, primary reference solutions with an expanded uncertainty associated with  
45 the mass fraction of less than 0.05 % are gravimetrically prepared and metrologically  
46 monitored by NMIs [2].

47 As the pure and fully characterized materials and the primary solutions have a limited  
48 availability and are very valuable concerning the characterization and preparation  
49 process, secondary solutions are prepared using pure materials usually only characterized  
50 regarding metallic impurities. Therefore, these secondary solutions must be linked up to  
51 the primary solutions. The expanded measurement uncertainty of the linkup must be less  
52 than 0.1 % to achieve a calibration measurement of commercial solutions with an  
53 expanded uncertainty associated with the mass fraction of 0.3 %. Overall, this procedure  
54 demonstrates an unbroken chain of calibrations to link up the measurement results in the  
55 field to the SI [3].

56 In this framework, high precision measurements are needed to link up the solutions with  
57 a relative expanded uncertainty of less than 0.1 %. In most cases, those measurements are  
58 being performed using the inductively coupled plasma optical emission spectrometry  
59 (ICP OES) technique.

60 Given that the application of instrumental neutron activation analysis (INAA) technique  
61 is missing in this field, a measurement procedure is suggested and the related  
62 measurement model is obtained from the neutron activation equation. In addition, the

63 proposed procedure was experimentally tested in the case of two Mo solutions having the  
64 same mass fraction, i.e. when the ratio is expected to be the unit value.

## 65 **Measurement procedure and model**

66 The aim of the measurement is to link up an elemental solution ES1 to an elemental  
67 solution ES2 having mass fractions  $w_{ES1}(E)$  and  $w_{ES2}(E)$  of an element E by determining  
68 the ratio

$$69 \quad \tau = \frac{w_{ES1}(E)}{w_{ES2}(E)} \quad (1)$$

70 with a relative expanded uncertainty of 0.1 %.

71 To accomplish this aim, two measurement solutions, mS1 and mS2, are stocked in two  
72 different containers by adding a sample (aliquot) of a monitor solution MS having a mass  
73 fraction  $w_{MS}(E_M)$  of a monitor element  $E_M$  to a sample of each elemental solution. Two  
74 sub-samples of the measurement solutions, mS1,s and mS2,s, are used in the neutron  
75 activation experiment.

76 To achieve the target uncertainty, attention has to be given to the evaporation of the  
77 solution during handling. The elemental solution starts to evaporate with a mass rate  $\alpha_{ES}$   
78 when it is transferred from its bottle to the container. After a time  $t_{MS}$ , the monitor  
79 solution is pipetted into the container to obtain the final measurement solution. The  
80 solution carries on evaporating during a time  $t_{ms}$ , with a mass rate  $\alpha_{mS}$ , until a sub-sample  
81 is taken and pipetted into an irradiation vial.

82 Hence, when the sub-samples are taken, the masses of the measurement solutions are  
83  $m_{mS1} = m_{ES1} - \alpha_{E1} t_{MS1} + m_{1,MS} - \alpha_{mS1} t_{mS1}$  and  $m_{mS2} = m_{ES2} - \alpha_{E2} t_{MS2} + m_{2,MS} - \alpha_{mS2} t_{mS2}$ ,  
84 where  $m_{ES1}$ ,  $m_{ES2}$  are the masses of the samples of ES1, ES2 and  $m_{1,MS}$ ,  $m_{2,MS}$  are the  
85 additional masses of MS.

86 The mass fractions of E and  $E_M$  in the measurement solutions are

$$87 \quad w_{mS1}(E) = \frac{w_{ES1}(E)}{1 + \frac{m_{1,MS} - m_{ev1}}{m_{ES1}}}, \quad w_{mS2}(E) = \frac{w_{ES2}(E)}{1 + \frac{m_{2,MS} - m_{ev2}}{m_{ES2}}} \quad (2)$$

88 and

$$89 \quad w_{mS1}(E_M) = \frac{w_{MS}(E_M)}{1 + \frac{m_{ES1} - m_{ev1}}{m_{1,MS}}}, \quad w_{mS2}(E_M) = \frac{w_{MS}(E_M)}{1 + \frac{m_{ES2} - m_{ev2}}{m_{2,MS}}}, \quad (3)$$

90 respectively, where  $m_{ev1} = \alpha_{E1} t_{MS1} + \alpha_{mS1} t_{mS1}$  and  $m_{ev2} = \alpha_{E2} t_{MS2} + \alpha_{mS2} t_{mS2}$  are the  
91 evaporated masses.

92 The number of atoms of an isotope  ${}^iE$  of E and of an isotope  ${}^iE_M$  of  $E_M$  in  $mS1,s$  and  
93  $mS2,s$  are

$$94 \quad n_{mS1,s}({}^iE) = \frac{x({}^iE) N_A w_{mS1}(E) m_{mS1,s}}{M(E)}, \quad n_{mS2,s}({}^iE) = \frac{x({}^iE) N_A w_{mS2}(E) m_{mS2,s}}{M(E)}, \quad (4)$$

95 and

$$96 \quad n_{mS1,s}({}^iE_M) = \frac{x({}^iE_M) N_A w_{mS1}(E_M) m_{mS1,s}}{M(E_M)}, \quad n_{mS2,s}({}^iE_M) = \frac{x({}^iE_M) N_A w_{mS2}(E_M) m_{mS2,s}}{M(E_M)}, \quad (5)$$

97 respectively, where  $m_{mS1,s}$  and  $m_{mS2,s}$  are the masses of  $mS1,s$  and  $mS2,s$ ,  $N_A$  is the  
98 Avogadro constant,  $x({}^iE)$  and  $x({}^iE_M)$  are the mole fractions of  ${}^iE$  and  ${}^iE_M$ ,  $M(E)$  and  
99  $M(E_M)$  are the molar masses of E and  $E_M$ , respectively. Here and hereafter the subscript  
100 M refers to the monitor element.

101 From (1), (2) and (4) it follows

$$102 \quad \tau = \frac{\left(1 + \frac{m_{1,MS} - m_{ev1}}{m_{ES1}}\right) \frac{n_{mS1,s}({}^iE)}{m_{mS1,s}}}{\left(1 + \frac{m_{2,MS} - m_{ev2}}{m_{ES2}}\right) \frac{n_{mS2,s}({}^iE)}{m_{mS2,s}}}. \quad (6)$$

103 The two sub-samples of the measurement solutions, mS1,s and mS2,s, are co-irradiated in  
 104 a neutron flux to activate the target isotopes  ${}^i\text{E}$  and  ${}^i\text{E}_\text{M}$ .

105 The counting of the  $\gamma$ -photons emitted during the radioactive decay of the radionuclide  
 106 produced by activation of the target isotope  ${}^i\text{E}$  allows to quantify the ratio

$$107 \quad \frac{n_{\text{mS1,s}}({}^i\text{E})}{n_{\text{mS2,s}}({}^i\text{E})} = \kappa_{\text{td}} \kappa_{\text{R}} \kappa_{\varepsilon} \kappa_{\text{ss}} \kappa_{\text{sa}} \kappa_{\text{g}} \frac{C_{\text{mS1,s}}(t_{\text{d mS1,s}})}{C_{\text{mS2,s}}(t_{\text{d mS2,s}})}, \quad (7)$$

108 where  $C(t_{\text{d}})$  is the full-energy  $\gamma$ -peak detection count rate at a time  $t_{\text{d}}$  after the end of the  
 109 irradiation; here and hereafter, the subscripts mS1,s and mS2,s are occasionally omitted  
 110 in  $C(t_{\text{d}})$ . The correction factors  $\kappa_{\text{td}} = e^{-\lambda(t_{\text{d mS2,s}} - t_{\text{d mS1,s}})}$ ,  $\kappa_{\text{R}} = R_{\text{mS2,s}}/R_{\text{mS1,s}}$ ,

111  $\kappa_{\varepsilon} = \varepsilon_{\text{mS2,s}}/\varepsilon_{\text{mS1,s}}$ ,  $\kappa_{\text{ss}} = k_{\text{ss mS2,s}}/k_{\text{ss mS1,s}}$ ,  $\kappa_{\text{sa}} = k_{\text{sa mS2,s}}/k_{\text{sa mS1,s}}$  and

112  $\kappa_{\text{g}} = k_{\text{g mS2,s}}/k_{\text{g mS1,s}}$  take the differences of decay time, reaction rate, detection  
 113 efficiency, self-shielding, self-absorption and geometry of the sub-samples into account.

114 In detail,  $\lambda$  is the decay constant of the produced radionuclide,  $R$  is the reaction rate per  
 115 target isotope  ${}^i\text{E}$ ,  $\varepsilon$  is the detection full-energy  $\gamma$  efficiency for a point-like source located  
 116 at the center of mass of the sub-sample,  $k_{\text{ss}}$ ,  $k_{\text{sa}}$ , and  $k_{\text{g}}$  are the neutron self-shielding, the  
 117 gamma self-absorption and the geometry factors, respectively.

118 It is worth to note that in the case of a radionuclide which emits  $\gamma$ -photons with several  
 119 energies  $E_{\gamma}$ , best results are achieved by using in (7) the mean value of the count rate

$$120 \quad \text{ratios, } \left. \frac{C_{\text{mS1,s}}(t_{\text{d mS1,s}})}{C_{\text{mS2,s}}(t_{\text{d mS2,s}})} \right|_{\text{m}}, \text{ obtained with different } E_{\gamma}.$$

121 The  $\gamma$ -counting is carried out using germanium detectors. The count rate  $C(t_{\text{d}})$  is obtained  
 122 by averaging  $n$  values,  $C_i(t_{\text{d}})$ , acquired in a  $\gamma$ -spectrometry sequence starting at a decay  
 123 time  $t_{\text{d}1}$  after the end of the irradiation and consisting of  $n$  consecutive counts performed  
 124 during the decay of the produced radionuclide. More explicitly, each  $i^{\text{th}}$  count rate value,  
 125  $C_i(t_{\text{d}})$ , extrapolated to  $t_{\text{d}}$  from the  $i^{\text{th}}$  count of the sequence, starting at  $t_{\text{d}i}$  and lasting  $t_{\text{c}i}$ , is

$$C_i(t_d) = \frac{\lambda n_{ci}}{e^{-\lambda(t_{di}-t_d)}(1-e^{-\lambda t_{ci}})} \frac{t_{ci}}{t_{ci}-t_{dead i}}, \quad (8)$$

where  $n_{ci}$  and  $t_{dead i}$  are the net count of the full-energy  $\gamma$ -peak and the detection dead time of the  $i^{\text{th}}$  count, respectively.

In the case of a  $1/E^{1+\alpha}$  epithermal spectrum and if the target isotope  $^i\text{E}$  is activated via a  $(n,\gamma)$  reaction having a cross section with a  $E^{-1/2}$  energy dependence, the reaction rate can be described using the Høgdahl convention [4],  $R = \Phi_{ep} \sigma_{0,E} (f + Q_{0,E}(\alpha))$ , where  $\Phi_{ep}$  is the epithermal neutron flux,  $f = \Phi_{th}/\Phi_{ep}$  is the thermal (sub-cadmium) to epithermal neutron flux ratio,  $\sigma_{0,E}$  is the  $(n,\gamma)$  cross section of  $^i\text{E}$  at 0.0253 eV and

$$Q_{0,E}(\alpha) = (Q_{0,E} - 0.429) \bar{E}_r^{-\alpha} + \frac{0.429}{(2\alpha + 1) 0.55^\alpha}. \quad (9)$$

In (9)  $Q_{0,E}$  is the ratio between the resonance integral of  $^i\text{E}$  for a  $1/E$  epithermal spectrum,  $I_{0,E}$ , and  $\sigma_{0,E}$ , and  $\bar{E}_r$  is the effective resonance energy of  $^i\text{E}$  [5].

Thus, the characteristics of the neutron energy spectrum affect the  $\kappa_R$  correction factor according to

$$\kappa_R = \frac{\Phi_{ep2}(f_2 + Q_{0,E}(\alpha_2))}{\Phi_{ep1}(f_1 + Q_{0,E}(\alpha_1))}, \quad (10)$$

where  $\Phi_{ep1}$ ,  $f_1$ ,  $\alpha_1$  and  $\Phi_{ep2}$ ,  $f_2$ ,  $\alpha_2$  are referred to the irradiation positions of mS1,s and mS2,s, respectively.

Several methods have been developed and used to measure the neutron flux parameters; as examples, (i) the “Cd-covered multi-monitor”, the “Cd-ratio for multi-monitor” and the “bare multi-monitor” methods for  $\alpha$ , (ii) the “Cd-ratio” for  $\Phi_{ep}$  and  $f$ , (iii) the “bare bi-isotopic monitor” method for  $f$  [5]. These methods are usually applied offline, i.e. before (or after) the experiment, by assuming that the neutron energy spectrum remains constant and do not depend on the irradiation samples.



148 In our case, since the  $\kappa_R$  value is required with a relative expanded uncertainty of less  
 149 than 0.1 %, online information is valuable. To reach this aim, the monitor solution is  
 150 added to the elemental solution. If the Høgdahl convention applies to the target isotope  
 151  ${}^i\text{E}_M$ ,

$$152 \quad \kappa_{M-R} = \frac{\Phi_{ep2}(f_2 + Q_{0,EM}(\alpha))}{\Phi_{ep1}(f_1 + Q_{0,EM}(\alpha))}. \quad (11)$$

153 From (10) and (11) it follows

$$154 \quad \kappa_R = \kappa_{M-R} \frac{1 + \frac{\alpha_Q Q_{0,E}(\alpha)}{f_1 + Q_{0,E}(\alpha)}}{1 + \frac{\alpha_Q Q_{0,E}(\alpha)}{f_1(1 + \alpha_f) + Q_{0,E}(\alpha)}}, \quad (12)$$

$$155 \quad \text{where } \alpha_Q = \frac{Q_{0,EM}(\alpha) - Q_{0,E}(\alpha)}{Q_{0,E}(\alpha)} \text{ and } \alpha_f = \frac{f_2 - f_1}{f_1}.$$

156 The counting of the  $\gamma$ -photons emitted during the radioactive decay of the radionuclide  
 157 produced by activation of the target isotope  ${}^i\text{E}_M$  allows to determine

$$158 \quad \kappa_{M-R} = (\kappa_{M-td} \kappa_{M-\varepsilon} \kappa_{M-ss} \kappa_{M-sa} \kappa_{M-g})^{-1} \frac{C_{M-mS2,s}(t_{dM-mS2,s}) n_{mS1,s}({}^i\text{E}_M)}{C_{M-mS1,s}(t_{dM-mS1,s}) n_{mS2,s}({}^i\text{E}_M)}. \quad (13)$$

159 According to (3) and (5), the ratio

$$160 \quad \frac{n_{mS1,s}({}^i\text{E}_M)}{n_{mS2,s}({}^i\text{E}_M)} = \frac{m_{mS1,s} \left( 1 + \frac{m_{ES2} - m_{ev2}}{m_{2,MS}} \right)}{m_{mS2,s} \left( 1 + \frac{m_{ES1} - m_{ev1}}{m_{1,MS}} \right)}. \quad (14)$$

161 In conclusion, the measurement model adopted to link up ES1 to ES2 is obtained from  
 162 (6), (7), (12), (13) and (14):

$$\begin{aligned}
 163 \quad \tau = & \frac{m_{ES2}}{m_{ES1}} \frac{m_{1,MS}}{m_{2,MS}} \frac{C_{mS1,s}(t_{d\ mS1,s})}{C_{mS2,s}(t_{d\ mS2,s})} \frac{C_{M-mS2,s}(t_{d\ M-mS2,s})}{C_{M-mS1,s}(t_{d\ M-mS1,s})} , \\
 & \times \beta_R \kappa_{td} \kappa_{M-td}^{-1} \kappa_{ss} \kappa_{M-ss}^{-1} \kappa_{sa} \kappa_{M-sa}^{-1} \kappa_g \kappa_{M-g}^{-1} \kappa_\varepsilon \kappa_{M-\varepsilon}^{-1}
 \end{aligned} \quad (15)$$

$$164 \quad \text{where } \beta_R = \frac{1 + \frac{\alpha_Q Q_{0,E}(\alpha)}{f_1 + Q_{0,E}(\alpha)}}{1 + \frac{\alpha_Q Q_{0,E}(\alpha)}{f_1(1 + \alpha_f) + Q_{0,E}(\alpha)}} .$$

165 It is remarkable that the result is independent on the masses of the evaporated solutions  
 166  $m_{ev1}$ ,  $m_{ev2}$ , on the masses of the irradiated sub-samples  $m_{mS1,s}$ ,  $m_{mS2,s}$  and on the  
 167 epithermal flux at the irradiation positions  $\Phi_{ep1}$ ,  $\Phi_{ep2}$ . Moreover, in case of (i) large  $f$ , (ii)  
 168  $Q_{0,EM}(\alpha) \cong Q_{0,E}(\alpha)$  or (iii)  $f_1 \cong f_2$ , the result becomes less affected by the  $f$ ,  $\alpha$ ,  $\bar{E}_r$ ,  $Q_{0,E}$ ,  
 169 and  $Q_{0,EM}$  values.

## 170 Experimental

171 The proposed procedure was tested using a Mo solution having a mass fraction  
 172  $w(\text{Mo}) \approx 1 \text{ g kg}^{-1}$ . In this preliminary experiment, a Co solution having a mass fraction  
 173  $w(\text{Co}) \approx 1 \text{ g kg}^{-1}$  was adopted as the monitor solution. The Mo and Co solutions were  
 174 obtained using ultrapure ammonium molybdate tetrahydrate,  $(\text{NH}_4)_6\text{Mo}_7\text{O}_{24} \cdot 4 \text{ H}_2\text{O}$ , in  
 175 water and ultrapure Co metal in  $0.5 \text{ mol L}^{-1}$  nitric acid, respectively.

176 A single measurement solution, mS, was prepared in a container by adding the Co  
 177 solution to the Mo solution. Two sub-samples were taken and used for the neutron  
 178 irradiation. This mimics the application of the procedure in the case of two Mo solutions  
 179 having the same mass fraction, i.e.  $w_{ES1}(E) = w_{ES2}(E)$ ,  $m_{ES1} = m_{ES2}$ ,  $m_{1,MS} = m_{2,MS}$ . To  
 180 attain the objective, (15) must be satisfied, i.e.  $\tau = 1$ , with a relative expanded  
 181 uncertainty of 0.1 %.

182 The  $\tau$  value was determined by counting (i) the 140.51 keV  $\gamma$ -photons emitted during the  
 183 radioactive decay of  $^{99}\text{Mo}$  and  $^{99m}\text{Tc}$  in equilibrium conditions and produced by

184 activation of  $^{98}\text{Mo}$  via the  $(n,\gamma)$  neutron capture reaction, and (ii) the 1173.23 keV and  
185 1332.49 keV  $\gamma$ -photons emitted during the radioactive decay of  $^{60}\text{Co}$  produced by  
186 activation of  $^{59}\text{Co}$  via the  $(n,\gamma)$  neutron capture reaction.

### 187 *Preparation of the measurement solution*

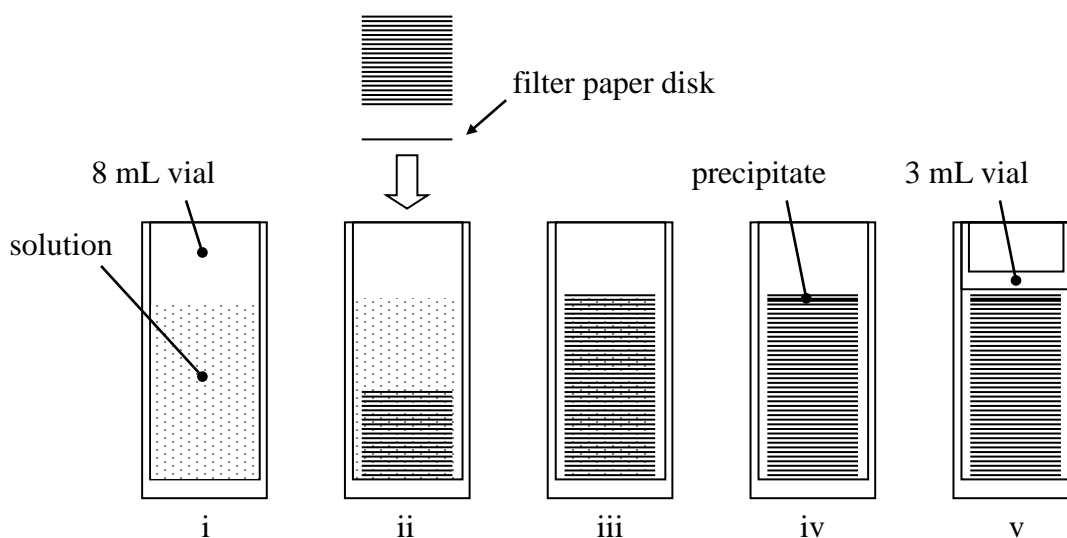
188 The measurement solution was prepared by pipetting the Co solution to a 25 mL  
189 polytetrafluoroethylene (PTFE) flask filled with the Mo solution. To correct for the effect  
190 of the evaporation, the mass of the measurement solution,  $m_{\text{MS}}$ , was recorded  
191 continuously during its preparation with a sampling frequency of 1 Hz. The data were  
192 collected using a digital analytical balance having a resolution of 0.01 mg and calibrated  
193 with SI-traceable weights. It is noteworthy that, although the buoyancy affects the  
194 weighing of the solution, the ratios of the masses in the model (15) eliminates the effect  
195 on  $\tau$ . Therefore, the weighed masses were not corrected for buoyancy.

196 The room temperature during the preparation was 26 °C. After setting to zero (tare) the  
197 reading of the balance with the empty flask, (i) 21 mL of Mo solution, (ii) 125  $\mu\text{L}$  of Co  
198 solution and (iii) 6 mL of Mo solution were consecutively added at 179 s, 532 s and  
199 993 s, respectively. The balance drift during the recording session was  $-0.02$  mg.

200 A straight line was fitted to the data collected between (i) 223 s and 524 s, (ii) 623 s and  
201 919 s, (iii) 1025 s and 1285 s. The evaporation rates were found to be  $2.1 \times 10^{-6} \text{ g s}^{-1}$ ,  
202  $2.0 \times 10^{-6} \text{ g s}^{-1}$  and  $3.3 \times 10^{-6} \text{ g s}^{-1}$ . According to the fitted data, the masses of the added  
203 solutions at steps (i), (ii) and (iii) were  $m_{\text{ES}} = 20.96218(4)$  g,  $m_{\text{MS}} = 0.12572(4)$  g and  
204  $m_{\text{ES}} = 6.07041(4)$  g, respectively. Here and hereafter, unless otherwise specified, the  
205 brackets refer to the standard uncertainty. The residuals of the fitted data were on average  
206 within  $\pm 0.02$  mg. However, since there are also spikes up to 0.04 mg, an uncertainty of  
207 0.04 mg was assigned to the measured masses.

### 208 *Preparation of the irradiation samples*

209 Two sub-samples, 2 mL volumes, of the measurement solution, hereafter called samples,  
210 were taken and pipetted in two different 8 mL polyethylene (PE) vials. Afterwards,  
211 80 filter paper disks (12 mm diameter) obtained from a single sheet using a cutting punch  
212 were inserted in both the PE vials. The paper disks were subsequently dried using an IR  
213 lamp and pressed using a slice of a 3 mL vial sealed to the 8 mL vial. It was assumed that  
214 the Mo and Co content of the pipetted solutions precipitates completely in the paper  
215 disks; this was confirmed by subsequent measurements with the emptied PE vials. The  
216 preparation of a sample for irradiation is summarized in Fig. 1.



217

218 **Fig. 1** Preparation of an irradiation sample; (i) the pipetted sub-sample of the  
219 measurement solution, (ii) and (iii) insertion of the filter paper disks, (iv) paper disks  
220 after drying, (v) sealed PE vial

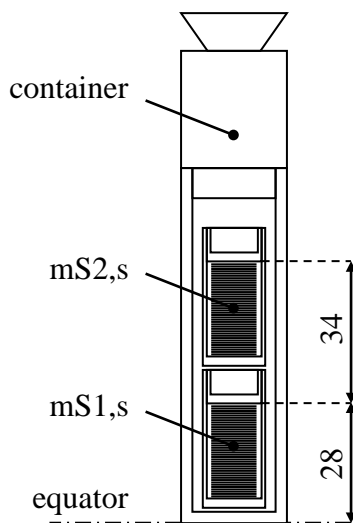
221 The visual inspection of the PE vials after drying was evidence for a precipitation largely  
222 occurring in the upper part of the piled disks (see the picture in Fig. S1). This was proof  
223 that the Mo and Co solutes were not homogeneously distributed in the paper disks. Since  
224 the mass fraction of the Co solution in the measurement solution was at  $10^{-3}$  level, the  
225 pipetted 2 mL solution consisted of 2 mg of Mo and the observed precipitate could have  
226 been ammonium molybdate tetrahydrate.

227 To limit the effect of external contaminations, the PE vials, the tweezers used to handle  
228 the filter paper disks were cleaned in an ultrasonic bath with diluted  $\text{HNO}_3$  and the  
229 cutting punch was washed with isopropyl alcohol. The water was purified using a

230 Millipore system ( $\rho \geq 18 \text{ M}\Omega$ ). Concerning the filter paper, a previous neutron activation  
231 experiment carried out with the disks did not show any contamination of Co and Mo.

232 *Neutron irradiation and gamma spectrometry*

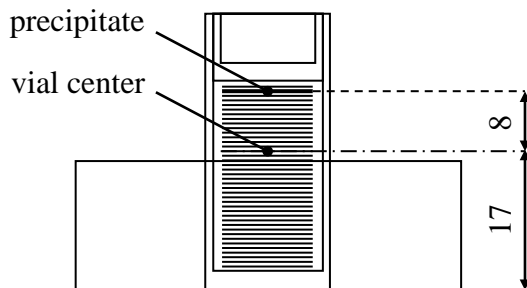
233 The neutron irradiation lasted 3 h and was performed in the central channel of the  
234 250 kW TRIGA Mark II reactor at the Laboratory of Applied Nuclear Energy (LENA) of  
235 the University of Pavia. The nominal thermal and epithermal neutron fluxes were about  
236  $6 \times 10^{12} \text{ cm}^{-2} \text{ s}^{-1}$  and  $5.5 \times 10^{11} \text{ cm}^{-2} \text{ s}^{-1}$ , resulting in a nominal  $f$  value of 10.9. The  
237 samples were put in a PE container used for irradiation. Fig. 2 shows the position of the  
238 container and the samples with respect to the equator of the reactor core.



239

240 **Fig. 2** Position of the irradiation container and the samples with respect to the equator of  
241 the reactor core; dimensions are in mm

242 After the neutron irradiation, the samples were extracted from the container, rinsed with  
243 diluted  $\text{HNO}_3$  and fixed to a  $\gamma$ -counting container (Fig. 3).

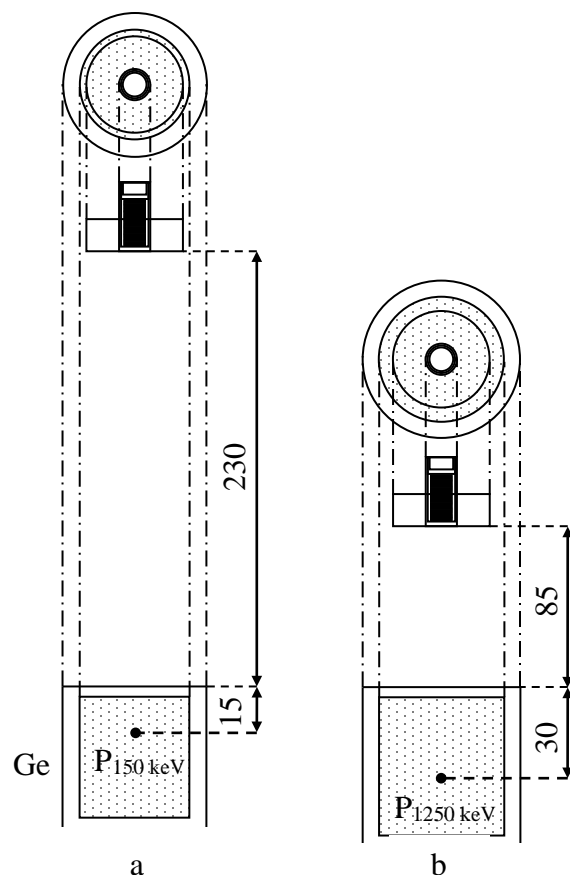


244

245 **Fig. 3** Position of the sample with respect to the  $\gamma$ -counting containers; dimensions are in  
246 mm

247 The  $\gamma$ -detection was carried out using a detector Canberra GC3518 (relative efficiency  
248 35 %, 1.80 keV FWHM resolution at 1332 keV), and a detector ORTEC<sup>®</sup> GEM50P4-83  
249 (66 mm crystal diameter, 50 % relative efficiency, 1.90 keV FWHM resolution at  
250 1332 keV).

251 Six  $\gamma$ -spectrometry sequences were recorded with a digital signal processor  
252 ORTEC<sup>®</sup> DSPEC 502 and a personal computer running the software for data acquisition  
253 ORTEC<sup>®</sup> Gamma Vision [6]. The first four sequences were performed with the GC3518  
254 and concerned the 140.51 keV  $\gamma$ -emission of <sup>99</sup>Mo and <sup>99m</sup>Tc in equilibrium conditions.  
255 The latter two  $\gamma$ -spectrometry sequences were performed with the GEM50P4-83 and  
256 concerned the 1173.23 keV and 1332.49 keV  $\gamma$ -emission of <sup>60</sup>Co. Each sequence  
257 consisted of  $n$  counts performed by adjusting on-line the counting window to reach a  
258 0.23 % counting uncertainty. The dead to counting time ratio,  $t_{\text{dead}}/t_c$ , of the detection  
259 systems during the data collection was always below 2.5 %. The position of the  $\gamma$ -  
260 counting containers with respect to the detector during the first four and the latter two  
261 sequences are displayed in Fig. 4a and Fig. 4b, respectively. In particular, the distances  
262 between the bottom of the  $\gamma$ -counting container and the end-cap of the detector were  
263  $d_{\text{GC3518}} = 230$  mm and  $d_{\text{GEM50P4-83}} = 85$  mm.



264  
 265 **Fig. 4** Position of the  $\gamma$ -counting containers (a) with respect to the detector GC3518  
 266 during  $^{99}\text{Mo}$  and  $^{99\text{m}}\text{Tc}$  detection and (b) with respect to the detector GEM50P4-83 during  
 267 the  $^{60}\text{Co}$  detection. The point  $P_{E\gamma}$  defines the (virtual) vertical position within the Ge  
 268 crystal where the detection efficiency  $\varepsilon$  tends to infinite; dimensions are in mm

269 The sequence number, the sample, the decay time at the beginning of the sequence,  $t_{d1}$ ,  
 270 and the number of collected counts,  $n$ , are summarized in table 1. The first sequence  
 271 started about 4 days after the end of the irradiation to assure a negligible effect due to the  
 272  $^{99}\text{Mo}$  and  $^{99\text{m}}\text{Tc}$  equilibrium conditions [5].

273 **Table 1** The sample, the decay time,  $t_{d1}$ , and the number of collected counts,  $n$ , in each  
 274 sequence

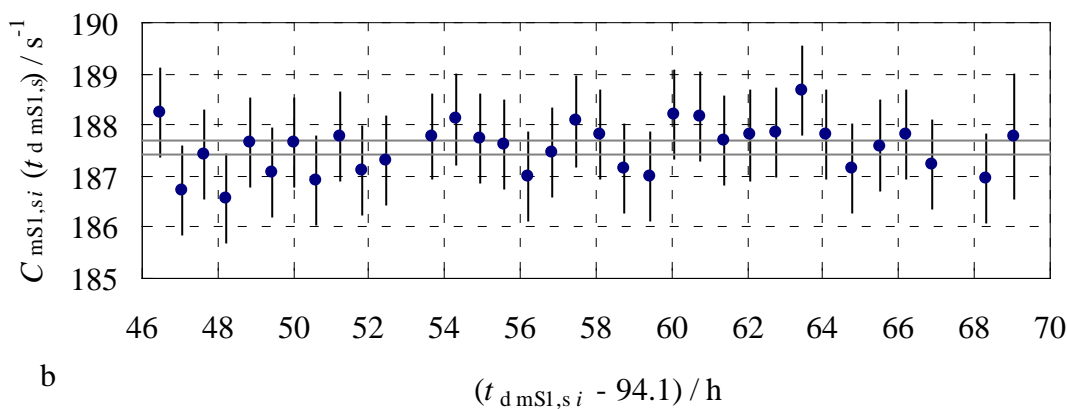
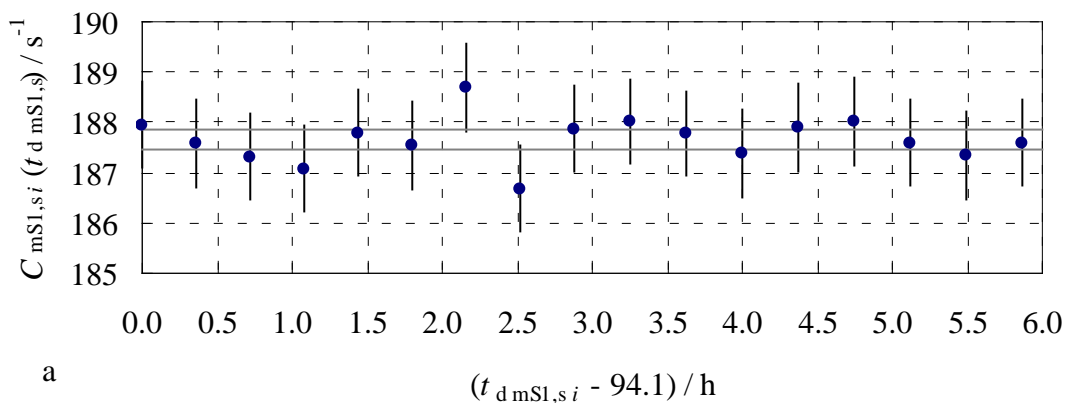
sequence	sample	$t_{d1}$ / h	counts / $n$
1	mS1,s	94.1	17
2	mS2,s	118.3	38
3	mS1,s	152.9	36
4	mS2,s	163.6	27

5	mS1,s	692	14
6	mS2,s	1058	22

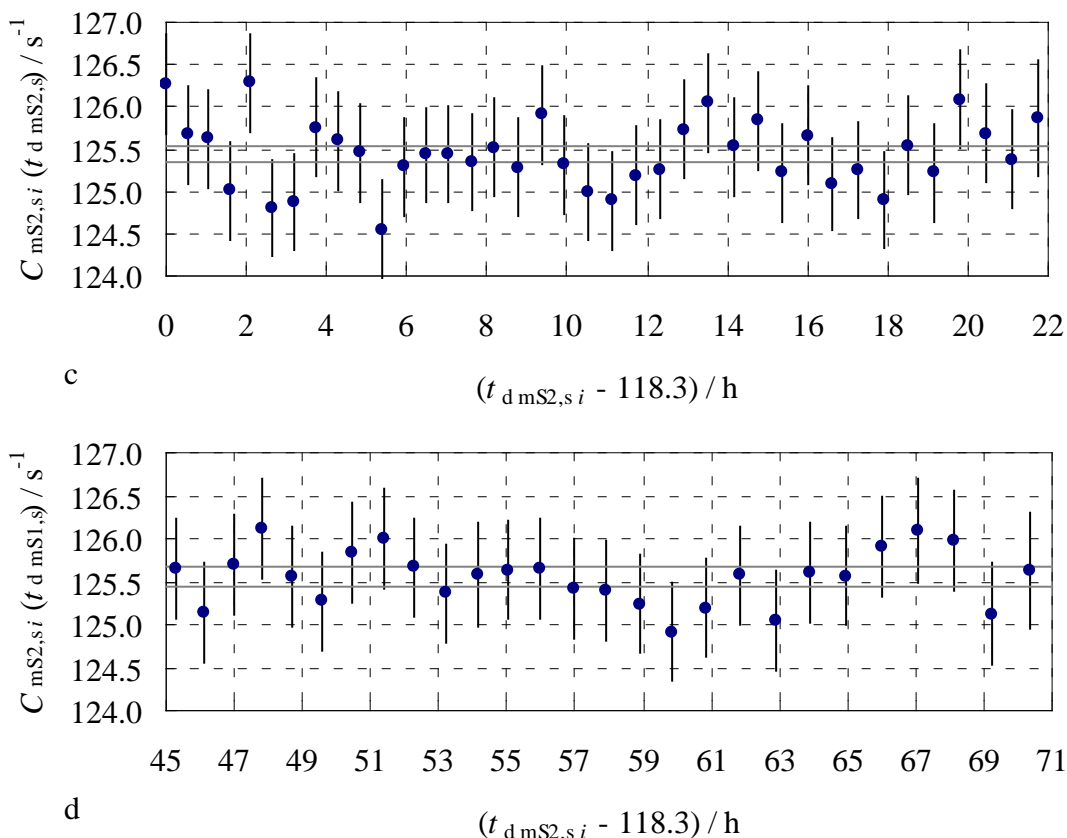
## 275 Results and discussion

276 The count rate of the  $i^{\text{th}}$  count of the sequence,  $C_i(t_d)$ , was computed according to (8). The  
 277 decay constants,  $\lambda = \ln(2) / t_{1/2}$ , were calculated using the half-life literature values, i.e.  
 278  $t_{1/2}({}^{99}\text{Mo}, {}^{99\text{m}}\text{Tc}) = 65.976(24) \text{ h}$  (in equilibrium conditions) and  
 279  $t_{1/2}({}^{60}\text{Co}) = 1925.28(14) \text{ d}$  [7, 8]. The net count,  $n_{c,i}$ , was obtained by fitting the full-  
 280 energy  $\gamma$ -peak with the algorithm implemented on the Gamma Vision software (analysis  
 281 engine wan32 G53W2.06).

282 The 140.51 keV  ${}^{99}\text{Mo}, {}^{99\text{m}}\text{Tc}$  count rates, extrapolated to  $t_{d \text{ mS1},s} = 94.1 \text{ h}$  and  
 283  $t_{d \text{ mS2},s} = 118.3 \text{ h}$ , are reported in Fig. 5. Here and hereafter, the error bars indicate the  
 284 95 % confidence interval due to counting statistics.





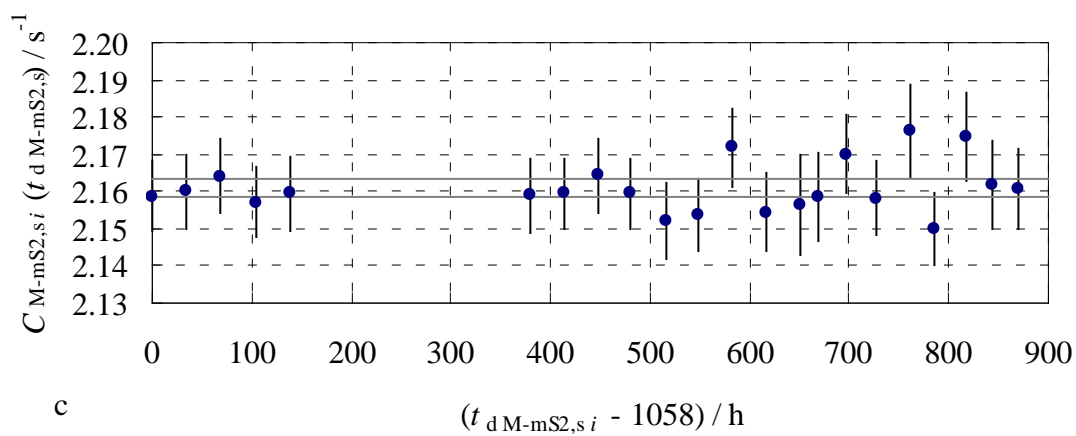
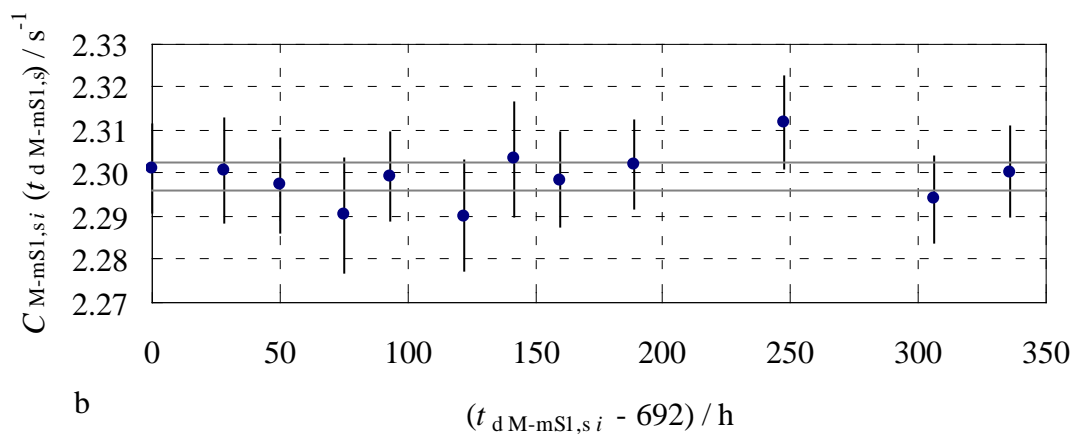
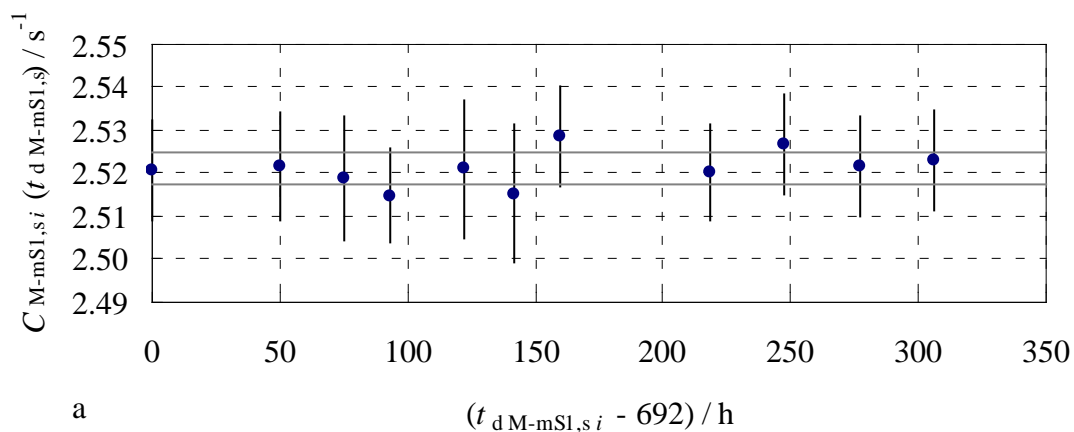


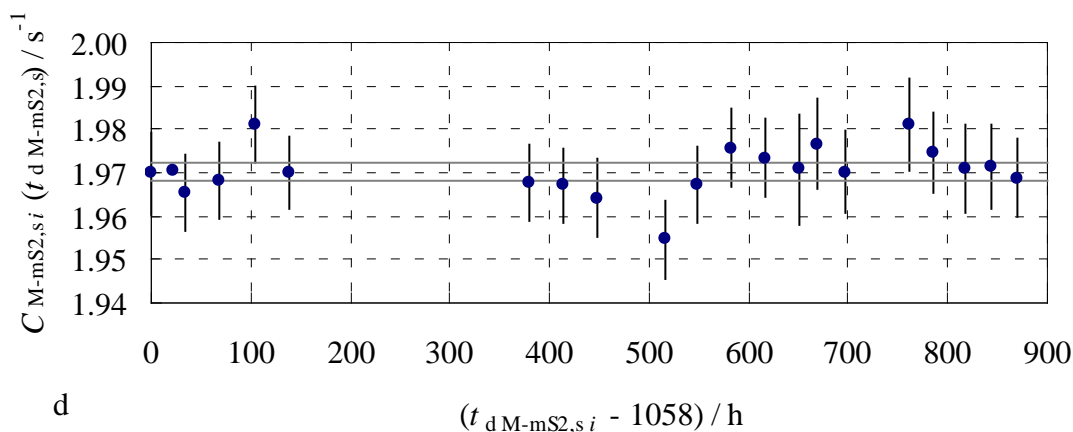
285 **Fig. 5** The 140.51 keV  $^{99}\text{Mo}$ ,  $^{99\text{m}}\text{Tc}$  count rates of the mS1,s sample extrapolated to  
 286  $t_{d\text{ mS1,s}} = 94.1$  h and recorded during (a) the sequence 1 and (b) the sequence 3. The  
 287 140.51 keV  $^{99}\text{Mo}$ ,  $^{99\text{m}}\text{Tc}$  count rates of the mS2,s sample extrapolated to  $t_{d\text{ mS2,s}} = 118.3$  h  
 288 and recorded during (c) the sequence 2 and (d) the sequence 4. The horizontal lines show  
 289 the 95 % confidence interval associated to the mean of the count rate values

290 The mean values of the 140.51 keV  $^{99}\text{Mo}$ ,  $^{99\text{m}}\text{Tc}$  count rates recorded with the mS1,s and  
 291 the mS2,s samples, extrapolated to  $t_{d\text{ mS1,s}} = 94.1$  h and  $t_{d\text{ mS2,s}} = 118.3$  h, were  
 292  $C_{\text{mS1,s}}(t_{d\text{ mS1,s}}) = 187.589(61) \text{ s}^{-1}$  and  $C_{\text{mS2,s}}(t_{d\text{ mS2,s}}) = 125.486(36) \text{ s}^{-1}$ , respectively  
 293 (uncertainties are due to counting statistics). The horizontal lines in Fig. 5 show the 95 %  
 294 confidence interval associated to the mean of the count rates values. The count rate ratio,

295 
$$\frac{C_{\text{mS1,s}}(t_{d\text{ mS1,s}})}{C_{\text{mS2,s}}(t_{d\text{ mS2,s}})},$$
 was  $1.49490(65) \text{ s}^{-1}$ .

296 The 1173.23 keV and 1332.49 keV  $^{60}\text{Co}$  count rates are reported in Fig. 6.





297 **Fig. 6** (a) The 1173.23 keV and (b) the 1332.49 keV  $^{60}\text{Co}$  count rates of the mS1,s  
 298 sample recorded during the sequence 5 and extrapolated to  $t_{d M-mS1,s} = 692$  h. (c) The  
 299 1173.23 keV and (d) the 1332.49 keV  $^{60}\text{Co}$  count rates of the mS2,s sample recorded  
 300 during the sequence 6 and extrapolated to  $t_{d M-mS2,s} = 1058$  h. The horizontal lines show  
 301 the 95 % confidence interval associated to the mean of the count rate values

302 The mean values of the 1173.23 keV  $^{60}\text{Co}$  count rates recorded with the mS1,s and the  
 303 mS2,s samples, extrapolated to  $t_{d M-mS1,s} = 692$  h and  $t_{d M-mS2,s} = 1058$  h, were  
 304  $C_{M-mS1,s}(t_{d M-mS1,s}) = 2.5212(19) s^{-1}$  and  $C_{M-mS2,s}(t_{d M-mS2,s}) = 2.1609(11) s^{-1}$ , respectively;  
 305 the mean values of the 1332.49 keV  $^{60}\text{Co}$  count rates recorded with the mS1,s and the  
 306 mS2,s samples, extrapolated to  $t_{d M-mS1,s} = 692$  h and  $t_{d M-mS2,s} = 1058$  h, were  
 307  $C_{M-mS1,s}(t_{d M-mS1,s}) = 2.2991(16) s^{-1}$  and  $C_{M-mS2,s}(t_{d M-mS2,s}) = 1.9704(10) s^{-1}$ , respectively  
 308 (uncertainties are due to counting statistics). The horizontal lines in Fig. 6 show the 95 %  
 309 confidence interval associated to the mean of the  $^{60}\text{Co}$  count rates values. The weighted

310 mean value of the count rate ratios,  $\left. \frac{C_{M-mS2,s}(t_{d M-mS2,s})}{C_{M-mS1,s}(t_{d M-mS1,s})} \right|_m$ , was  $0.85708(55) s^{-1}$ .

### 311 Correction Factors

312 The differences  $t_{d mS2,s} - t_{d mS1,s}$  and  $t_{d M-mS2,s} - t_{d M-mS1,s}$  were 24.2 h and 366 h,  
 313 respectively, i.e. about 0.4 times  $t_{1/2}(^{99}\text{Mo}, ^{99m}\text{Tc})$  and  $8 \times 10^{-3}$  times  $t_{1/2}(^{60}\text{Co})$ .  
 314 Accordingly,  $\kappa_{td} = 0.77554$  and  $\kappa_{M-td} = 0.99452$  with negligible uncertainties.

315 The measurement solutions had a similar Mo and Co mass fraction and the pipetted  
 316 subsamples had the same volume. In the case of a 1 mm thick, 12 mm diameter sample  
 317 with 2 mg Mo and 10  $\mu\text{g}$  Co, the neutron self-shielding factor is 0.998 for Mo and 1.000  
 318 for Co, i.e. 0.2 % epithermal neutron self-shielding for Mo. Even if the solutes were not  
 319 uniformly distributed in the paper disks, the neutron self-shielding factors  
 320  $k_{\text{ss mS1,s}} = k_{\text{ss mS2,s}}$ ,  $k_{\text{M-ss mS1,s}} = k_{\text{M-ss mS2,s}}$ . Similarly, the  $\gamma$ -self-absorption factors  
 321  $k_{\text{sa mS1,s}} = k_{\text{sa mS2,s}}$ ,  $k_{\text{M-sa mS1,s}} = k_{\text{M-sa mS2,s}}$  and the geometry factors  $k_{\text{g mS1,s}} = k_{\text{g mS2,s}}$ ,  
 322  $k_{\text{M-g mS1,s}} = k_{\text{M-g mS2,s}}$ . Thus,  $\kappa_{\text{ss}} = \kappa_{\text{M-ss}}^{-1} = \kappa_{\text{sa}} = \kappa_{\text{M-sa}}^{-1} = \kappa_{\text{g}} = \kappa_{\text{M-g}}^{-1} = 1$  with negligible  
 323 uncertainty.

324 The full-energy  $\gamma$ -peak detection efficiency  $\varepsilon$  tends to infinite in a (virtual) vertical  
 325 position within the Ge crystal of the detector [9]. This position depends on the  $\gamma$ -photon  
 326 energy,  $E_\gamma$ , and is defined by a point,  $\text{P}_{E_\gamma}$  (see Fig. 4). A previous characterization of the  
 327 detectors showed that the distance between the end-cap and  $\text{P}_{E_\gamma}$  is  $d_{150\text{ keV}} = 15$  mm for  
 328 the GC3518 and  $d_{1250\text{ keV}} = 30$  mm for the GEM50P4-83. The distance between the center  
 329 of the PE vial and the bottom of the  $\gamma$ -counting container,  $d_c$ , and the distance between  
 330 the center of the PE vial and the precipitate,  $d_p$ , were 17 mm and 8 mm, respectively (see  
 331 Fig. 3). The detection efficiency correction factors are

$$332 \quad \kappa_\varepsilon = \frac{(d_{\text{Mo}} + \Delta d_{\text{Mo2}})^2}{(d_{\text{Mo}} + \Delta d_{\text{Mo1}})^2} \quad \text{and} \quad \kappa_{\text{M-}\varepsilon} = \frac{(d_{\text{Co}} + \Delta d_{\text{Co2}})^2}{(d_{\text{Co}} + \Delta d_{\text{Co1}})^2}, \quad (16)$$

333 where  $\Delta d_{\text{Mo1}}$  and  $\Delta d_{\text{Mo2}}$  are the distances between the Mo center of mass and the center  
 334 of the PE vial in sample 1 and 2,  $\Delta d_{\text{Co1}}$  and  $\Delta d_{\text{Co2}}$  are the distances between the  
 335 Co center of mass and the center of the PE vial in sample 1 and 2,  
 336  $d_{\text{Mo}} = d_{150\text{ keV}} + d_{\text{GC3518}} + d_c = 262$  mm and  $d_{\text{Co}} = d_{1250\text{ keV}} + d_{\text{GEM50P4-83}} + d_c = 132$  mm.  
 337 As examples, if in both the samples all the Mo and Co were in the precipitate, i.e.  
 338  $\Delta d_{\text{Mo1}} = \Delta d_{\text{Mo2}} = \Delta d_{\text{Co1}} = \Delta d_{\text{Co2}} = d_p$ ,  $\kappa_\varepsilon = \kappa_{\text{M-}\varepsilon}^{-1} = 1$ . Instead, if in sample 2 only a  
 339 fraction of Mo and Co was in the precipitate, i.e.  $\Delta d_{\text{Mo1}} = \Delta d_{\text{Co1}} = d_p$  and  
 340  $\Delta d_{\text{Mo2}} = \Delta d_{\text{Co2}} = d_p - \Delta d_p$ , in the case of  $\Delta d_p = 4$  mm,  $\kappa_\varepsilon = 0.985$  and  $\kappa_{\text{M-}\varepsilon} = 0.971$ .

341 Since the actual positions of Mo and Co centers of mass were not measured,  
 342  $\Delta d_p = \pm 4$  mm (uniform distribution) was preliminary assigned. Accordingly,  
 343  $\kappa_\varepsilon = 1.000(9)$  and  $\kappa_{M-\varepsilon} = 1.000(16)$ .

344 The literature  $Q_0$  values for  $^{98}\text{Mo}$  and  $^{59}\text{Co}$  are 53.1(33) and 1.993(60) [10]. Experimental  
 345 data for the  $\alpha$  value at the LENA irradiation channel are missing. However, based on the  
 346  $\alpha = -0.051(8)$  value at the central channel of the TRIGA Mark II reactor operating in  
 347 Ljubljana [11], from (9) it follows that  $Q_{0,\text{Mo}}(\alpha) = 70(9)$ ,  $Q_{0,\text{Co}}(-0.051) = 2.5(6)$  and  
 348  $\alpha_Q = -0.965(10)$ .

349 Due to the 10.9 nominal  $f$  value, about 85% of the  $^{60}\text{Co}$  activity was produced by thermal  
 350 neutrons. As the  $^{60}\text{Co}$  count rate of sample 2 to the count rate of sample 1 ratio was about  
 351 0.86, the  $\Phi_{\text{th1}}$  was approximately 16 % higher than  $\Phi_{\text{th2}}$  and a possible variation of  $f$  could  
 352 be expected. In the case of  $\alpha_f = \pm 0.025$  (uniform distribution) and 10 % relative  
 353 uncertainty for the  $f$  value,  $\beta_R = 1.000(10)$ .

### 354 *Uncertainty budget*

355 The application of (15) to the experimental data collected in this study gave a ratio  
 356  $\tau = 0.999(19)$ . The provisional uncertainty budget calculated according to the Guide to  
 357 the Expression of Uncertainty in Measurement [12] is reported in table 2.

358 **Table 2** Uncertainty budget of the measured ratio  $\tau$ . The input quantities  $x_i$  are given in  
 359 the text. The index column gives the relative contributions of  $u(x_i)$  to the combined  
 360 standard uncertainty,  $u_c(y)$ , of  $\tau$

Quantity	Unit	Value	Standard uncertainty	Index
$X_i$	$[X_i]$	$x_i$	$u(x_i)$	%
$m_{1,\text{MS}}$	g	0.12572	0.00004	0.0
$m_{2,\text{MS}}$	g	0.12572	0.00004	0.0
$m_{\text{ES1}}$	g	27.03259	0.00006	0.0

$m_{ES2}$	g	27.03259	0.00006	0.0
$C_{mS1,s}/C_{mS2,s}$	1	1.49490	0.00065	0.0
$C_{M-mS2,s}/C_{M-mS1,s}$	1	0.85708	0.00055	0.1
$\beta_R$	1	1.000	0.010	22.8
$\kappa_{td}$	1	0.77554	0.00000	0.0
$\kappa_{M-td}$	1	0.99452	0.00000	0.0
$\kappa_{ss} (\kappa_{M-ss})^{-1}$	1	1.00000	0.00000	0.0
$\kappa_{sa} (\kappa_{M-sa})^{-1}$	1	1.00000	0.00000	0.0
$\kappa_g (\kappa_{M-g})^{-1}$	1	1.00000	0.00000	0.0
$\kappa_\varepsilon$	1	1.000	0.009	18.5
$\kappa_{M-\varepsilon}$	1	1.000	0.016	58.5
$Y$	[Y]	y	$u_c(y)$	
$\tau$	1	0.999	0.019	100.0

361 Given that the variation of the shape of the neutron energy spectrum and the detection  
 362 efficiency were the main influence factors, the following ways are suggested to reduce  
 363 their effects.

364 In particular, the measurement model shows that the adoption of a monitor element  
 365 having a  $Q_0$  value similar to the  $Q_0$  value of  $^{99}\text{Mo}$  makes the result almost independent on  
 366  $f$ ,  $\alpha$ ,  $Q_{0,E}$ , and  $Q_{0,EM}$  values. The best choice among the potential target elements is the  
 367  $^{116}\text{Sn}$ , which is neutron activated to  $^{117}\text{Sn}$  via (n, $\gamma$ ) capture reaction and detected via the  
 368 158.56 keV  $\gamma$ -photons emitted during the radioactive decay of  $^{117}\text{Sn}$  ( $t_{1/2} = 13.76(4)$  d  
 369 [13]). The outcome of the  $Q_0 = 56.3(11)$  value [10] of  $^{116}\text{Sn}$  might be a  $\beta_R = 1$  with a  
 370 relative uncertainty below 0.01 %.

371 Moreover, the actual position of the radionuclide center of mass with respect to the center  
 372 of the 8 mL PE vial can be experimentally determined by counting the sample right-side-  
 373 up and up-side-down. See equation (S1) in the supplementary information for detail.  
 374 Hence, the knowledge of the  $\Delta d_p$  value and the increase of the distance of the samples

375 from the detector during the  $\gamma$ -counting might limit the  $\kappa_{\varepsilon}$  and  $\kappa_{M-\varepsilon}$  relative uncertainty  
376 below 0.1 %.

## 377 **Conclusions**

378 The possibility of using the INAA technique to determine the ratio of the mass fractions  
379 of two mono-elemental solutions with a relative expanded uncertainty of less than 0.1 %  
380 was investigated. To reach the target uncertainty, the addition of a monitor solution to the  
381 elemental solution was essential to correct for possible variation of the neutron energy  
382 spectrum at the irradiation positions. A procedure was developed and the related  
383 measurement model was obtained from the neutron activation equation.

384 The proposed measurement procedure was applied in a feasibility test in the case of two  
385 Mo solutions having the same mass fraction, i.e. obtained from the same solution, and  
386 using Co as the monitor element. The departure of the measured ratio from the unit value  
387 (-0.1 %) was in agreement with the evaluated 1.9 % relative uncertainty. The uncertainty  
388 budget pointed out that the main contributors were the variation of the shape of the  
389 neutron energy spectrum and the detection efficiency.

390 The target 0.1 % relative expanded uncertainty was not achieved. Nevertheless, the use of  
391 INAA to link up Mo solutions to the SI is promising; a considerable decrease of the  
392 measurement uncertainty might be reached by improved sample preparation and an  
393 improved  $\gamma$ -counting technique.

## 394 **Acknowledgements**

395 Financial support by the European Metrology Research Programme (EMRP) is gratefully  
396 acknowledged (EMRP-SIB09 “Purity standards for challenging elements”) [14]. The  
397 EMRP is jointly funded by the EMRP participating countries within the European  
398 Association of National Metrology Institutes (EURAMET). The authors are grateful to  
399 the referee for providing constructive comments and help in improving the contents of  
400 this paper.

401        **References**

- 402    1. D'Agostino G, Bergamaschi L, Giordani L, Oddone M, Kipphardt H, Richter S (2014)  
403        Use of Instrumental Neutron Activation Analysis to investigate the distribution of  
404        trace elements among subsamples of solid materials. *Metrologia* 51:48-53
- 405    2. Kaltenbach A, Noordmann J, Görlitz V, Pape C, Richter S, Kipphardt H, Kopp G,  
406        Jährling R, Rienitz O, Güttler B (2015) Gravimetric preparation and characterization  
407        of primary reference solutions of molybdenum and rhodium. *Anal Bioanal Chem*  
408        407:3093-3102
- 409    3. Rienitz O, Schiel D, Görlitz V, Jährling R, Vogl J, Lara-Manzano J V, Zoń A, Fung W  
410        H, Buzoianu M, Caciano de Sena R, Augusto dos Reis L, Valiente L, Yim Y H, Hill S,  
411        Champion R, Fiscaro P, Bing W, Turk G C, Winchester M R, Saxby D, Merrick J,  
412        Hioki A, Miura T, Suzuki T, Linsky M, Barzev A, Máriássy M, Cankur O, Ari B,  
413        Tunç M, Konopelko L A, Kustikov Y A, Bezruchko M (2012) Final report on CCQM-  
414        K87: Mono-elemental calibration solutions. *Metrologia* DOI 10.1088/0026-  
415        1394/49/1A/08010
- 416    4. Høgdahl OT (1965) Proceedings of the Symposium on Radiochemical Methods of  
417        Analysis 1:23-40
- 418    5. De Corte F (1987) The  $k_0$ -Standardisation Method. A move to the optimization of  
419        Neutron Activation Analysis. Ed. Ryksuniversiteit Gent Faculteit Van de  
420        Wettenschappen
- 421    6. GammaVision (2006) Version 6.08; Advanced Measurement Technology, Inc.:  
422        Berwyn, PA
- 423    7. Browne E, Tuli J K (2011) *Nucl Data Sheets* 112:275-446
- 424    8. Browne E, Tuli J K (2013) *Nucl Data Sheets* 114:1849-2022
- 425    9. Gilmore G, Hemingway J D (1995) *Practical Gamma-ray Spectrometry*, New York,  
426        Wiley
- 427    10. Kolotov VP, De Corte F (2004) Compilation of  $k_0$  and related data for NAA in the  
428        form of electronic database (IUPAC Technical Report). *Pure Appl. Chem.* 76:1921-  
429        1925



- 430 11. Jovanovic S, Vukotic P, Smodis B, Jacimovic R, Mihaljevic N, Stegnar P (1989)  
431 Epithermal neutron flux characterization of the TRIGA Mark II reactor, Ljubljana,  
432 Yugoslavia, for use in NAA. J. Radioanal. Nucl. Chem. 129:343-349  
433 12. JGCM 100:2008 (2008) Evaluation of measurement data - Guide to the expression of  
434 uncertainty in measurement  
435 13. Blachot J (2002) Nucl Data Sheets 95:679-836  
436 14. Online available at <http://www.ptb.de/emrp/sib09.html>

## 437 **Supplementary information**

### 438 *Irradiation samples*



439

440 **Fig. S1** The precipitates in the upper part of the piled disks of the PE vials after drying

### 441 *Position of the radionuclide center of mass*

442 The distance between the radionuclide center of mass with respect to the center of the  
443 8 mL PE vial,  $\Delta d$ , can be determined by using the following formula:

444

$$\frac{C_{\text{rsu}}(t_d)}{C_{\text{usd}}(t_d)} = \frac{1 - \frac{\Delta d}{d}}{1 + \frac{\Delta d}{d}}, \quad (\text{S1})$$

445 where  $C_{\text{rsu}}(t_d)$ ,  $C_{\text{rsd}}(t_d)$  are the count rates recorded with the right-side-up and up-side-  
446 down sample, respectively, and  $d$  is the distance between the center of the 8 mL PE vial  
447 and the (virtual) vertical position where the detector efficiency tends to infinite.